Epstein–Barr virus nuclear antigen 2 extensively rewires the human chromatin landscape at autoimmune risk loci

Ted Hong, Sreeja Parameswaran, Omer A. Donmez, et al.

Genome Res. 2021 31: 2185-2198 originally published online November 19, 2021
Access the most recent version at doi:10.1101/gr.264705.120

Research

Epstein–Barr virus nuclear antigen 2 extensively rewires the human chromatin landscape at autoimmune risk loci

Ted Hong,[1,2,11,12] Sreeja Parameswaran,[1,11] Omer A. Donmez,[1] Daniel Miller,[1] Carmy Forney,[1] Michael Lape,[1,3] Mariana Saint Just Ribeiro,[1] Jun Liang,[4] Lee E. Edsall,[1] Albert F. Magnusen,[5] William Miller,[6] Iouri Chepelev,[1,7] John B. Harley,[1,7,8] Bo Zhao,[4] Leah C. Kottyan,[1,7,9] and Matthew T. Weirauch[1,3,7,10]

[1]*Center for Autoimmune Genomics and Etiology, Cincinnati Children's Hospital Medical Center, Cincinnati, Ohio 45229, USA;* [2]*Department of Pharmacology and Systems Physiology, University of Cincinnati, College of Medicine, Cincinnati, Ohio 45229, USA;* [3]*Division of Biomedical Informatics, Cincinnati Children's Hospital Medical Center, Cincinnati, Ohio 45229, USA;* [4]*Department of Medicine, Brigham and Women's Hospital, Harvard Medical School, Boston, Massachusetts 02115, USA;* [5]*Division of Human Genetics, Cincinnati Children's Hospital Medical Center, Cincinnati, Ohio 45229, USA;* [6]*Department of Molecular Genetics, Biochemistry, and Microbiology, University of Cincinnati, College of Medicine, Cincinnati, Ohio 45267, USA;* [7]*Department of Pediatrics, University of Cincinnati, College of Medicine, Cincinnati, Ohio 45229, USA;* [8]*US Department of Veterans Affairs Medical Center, Cincinnati, Ohio 45229, USA;* [9]*Division of Allergy and Immunology, Cincinnati Children's Hospital Medical Center, Cincinnati, Ohio 45229, USA;* [10]*Division of Developmental Biology, Cincinnati Children's Hospital Medical Center, Cincinnati, Ohio 45229, USA*

The interplay between environmental and genetic factors plays a key role in the development of many autoimmune diseases. In particular, the Epstein–Barr virus (EBV) is an established contributor to multiple sclerosis, lupus, and other disorders. Previously, we showed that the EBV nuclear antigen 2 (EBNA2) transactivating protein occupies up to half of the risk loci for a set of seven autoimmune disorders. To further examine the mechanistic roles played by EBNA2 at these loci on a genome-wide scale, we globally examined gene expression, chromatin accessibility, chromatin looping, and EBNA2 binding in a B cell line that was (1) uninfected, (2) infected with a strain of EBV lacking EBNA2, or (3) infected with a strain that expresses EBNA2. We identified more than 400 EBNA2-dependent differentially expressed human genes and more than 5000 EBNA2 binding events in the human genome. ATAC-seq analysis revealed more than 2000 regions in the human genome with EBNA2-dependent chromatin accessibility, and HiChIP data revealed more than 1700 regions where EBNA2 altered chromatin looping interactions. Autoimmune genetic risk loci were highly enriched at the sites of these EBNA2-dependent chromatin-altering events. We present examples of autoimmune risk genotype–dependent EBNA2 events, nominating genetic risk mechanisms for autoimmune risk loci such as *ZMIZ1*. Taken together, our results reveal important interactions between host genetic variation and EBNA2-driven disease mechanisms. Further, our study highlights a critical role for EBNA2 in rewiring human gene regulatory programs through rearrangement of the chromatin landscape and nominates these interactions as components of genetic mechanisms that influence the risk of multiple autoimmune diseases.

[Supplemental material is available for this article.]

Cross talk between genetic risk polymorphisms and environmental factors is thought to influence the onset and progression of many human diseases (Hunter 2005; Bookman et al. 2011; McAllister et al. 2017). Many diseases have a complex genetic etiology, including cancers (Flavahan et al. 2017), cardiovascular diseases (North et al. 2003), and autoimmune diseases such as multiple sclerosis (MS) (Ascherio and Munger 2007) and systemic lupus erythematosus (SLE) (Kamen 2014). Over the last 15 years, a multitude of genome-wide association studies (GWASs) have identified more than 50,000 disease-associated genetic variants for many disorders (Tam et al. 2019). As many as 90% of disease-associated genetic variants fall within noncoding regions of the genome (Hindorff et al. 2009; Maurano et al. 2012), implicating a key role for regulatory proteins such as transcription factors (TFs) in the etiology of human disease (Lee and Young 2013; Deplancke et al. 2016). Regulatory proteins bind to promoter regions and distal regions of target genes (e.g., enhancers) to alter gene expression through numerous mechanisms (for reviews, see Lambert et al. 2018; Sullivan et al. 2018; Schoenfelder and Fraser 2019). Some regulatory proteins, such as the pioneer factor EBF1,

[11]Co-first authors.
[12]Present address: Translational Medicine, R&D Oncology, AstraZeneca, Boston, MA 02451, USA
Corresponding authors: Leah.Kottyan@cchmc.org, Matthew.Weirauch@cchmc.org

Article published online before print. Article, supplemental material, and publication date are at https://www.genome.org/cgi/doi/10.1101/gr.264705.120. Freely available online through the *Genome Research* Open Access option.

are capable of directly altering the chromatin landscape. Other TFs, such as YY1 and CTCF, can affect the three-dimensional structure of chromatin by facilitating the formation of novel chromatin loops that alter gene transcription (Beagan et al. 2017; Weintraub et al. 2017). Thus, regulatory proteins likely can contribute to human disease processes through a variety of mechanisms.

Viral infections are a common environmental exposure known to be closely linked to many human diseases (Bray et al. 1983; Foxman and Iwasaki 2011; Hong et al. 2014; Pender and Burrows 2014). In particular, previous studies have revealed causative roles for the Epstein–Barr virus (EBV) in mononucleosis (Dunmire et al. 2015), Burkitt's lymphoma (Rochford and Moormann 2015), and Hodgkin lymphoma (Vockerodt et al. 2014). EBV is also strongly implicated in autoimmune diseases such as rheumatoid arthritis (RA) (Balandraud and Roudier 2018), inflammatory bowel disease (IBD) (Dimitroulia et al. 2013), SLE (Harley and James 2006), and MS (Bagert 2009). Despite extensive epidemiologic and serological evidence, the molecular mechanisms through which EBV-host interactions increase autoimmune disease risk remain largely unknown.

Viruses can directly perturb the host's transcriptome through the actions of virus-encoded transcriptional regulatory proteins (Agudelo-Romero et al. 2008; Clyde and Glaunsinger 2010; Bermudez-Morales et al. 2011; Graham 2016; Harley et al. 2018; Liu et al. 2020). Viral transcriptional regulators can either interact with the host genome directly, as is the case for the EBV-encoded Zta protein (Flemington and Speck 1990; Mahot et al. 2003), or indirectly through interactions with host DNA binding factors, such as the EBV-encoded Epstein–Barr virus nuclear antigen 2 (EBNA2) protein and the human TF RBPJ (Henkel et al. 1994). In both cases, genetic variation in the host genome can affect these virus–host interactions, leading to alteration of host gene expression levels (Bochkov et al. 2010; Çalışkan et al. 2015; Harley et al. 2018).

EBNA2 controls multiple processes, including the immortalization of EBV-infected B cells, by altering the expression levels of human genes (Pich et al. 2019). Mechanistically, EBNA2 mediates at least some of this regulation through interactions with human TFs such as RBPJ, SPI1 (also known as PU.1), and EBF1 (Zhao et al. 2011). The EBF1 protein can bind to and open chromatin that is occupied by EBNA2-RBPJ complexes (Lu et al. 2016). EBNA2 can also recruit chromatin remodelers such as the histone acetyltransferases EP300 and CREBBP (Lu et al. 2016; Wang et al. 2000) and the SWI/SNF complex (Wu et al. 2000), further supporting a role for EBNA2 in human chromatin rearrangement. Likewise, the EBNA2-RBPJ complex can create a new chromatin looping interaction between a distal enhancer region and the *MYC* promoter, inducing *MYC* expression that leads to continuous B cell proliferation (Zhao et al. 2011; Wood et al. 2016; Jiang et al. 2017). Despite these strong independent lines of evidence implicating EBNA2 in the alteration of chromatin accessibility and looping in the human genome, a genome-wide investigation of EBNA2-dependent human chromatin alteration has not been previously performed.

A recent study from our group revealed that a significant number of autoimmune disease–associated genetic loci contain genetic variants that are located within EBNA2 ChIP-seq peaks (Harley et al. 2018). In particular, nearly half of the SLE and MS genetic risk loci contain disease-associated genetic variants that are directly located within regions of the human genome occupied by EBNA2. We also discovered numerous examples of autoimmune-associated genetic variants that alter the binding of EBNA2 and other transcriptional regulators to the human genome in a genotype-dependent manner. Collectively, these results are consistent with EBNA2 playing an important role in autoimmune disease etiology.

Understanding the molecular mechanisms mediating interactions between EBNA2 and the human genome is important for achieving an understanding of the development and progression of autoimmune diseases. In our previous study, analysis of public data sets revealed the presence of EBNA2 ChIP-seq peaks at up to half of the risk loci for particular autoimmune diseases. In this study, we explore the role of EBNA2 within the human B cell gene regulatory network by examining EBNA2-dependent alterations to the human chromatin landscape and investigating the impact of autoimmune disease–associated genetic polymorphisms on these mechanisms. To identify EBNA2-dependent effects, we use an experimental design comparing human B cells that are (1) uninfected, (2) infected with an EBV strain (P3HR-1) that lacks EBNA2 (EBV^{EBNA2-}), or (3) infected with an EBV strain (B95.8) that has EBNA2 (EBV^{EBNA2+}). Using this approach, we identify human genes whose expression level changes coincide with the presence of EBNA2 (RNA-seq), and we resolve the effects of EBNA2 on chromatin accessibility (ATAC-seq) and chromatin looping (HiChIP). Further, we examine the enrichment of autoimmune disease risk genetic variants within these EBNA2-dependent regulatory mechanisms and identify allele-dependent EBNA2 behavior at autoimmune-associated variants.

Results

EBNA2 modulates human gene expression in EBV-infected B cells

To globally measure the effect of EBNA2 on human gene expression patterns, we performed RNA-seq in Ramos B cells in three experimental conditions: uninfected, EBV^{EBNA2-}, and EBV^{EBNA2+} (Fig. 1). We used the P3HR-1 EBV strain, which contains a naturally occurring EBNA2 deletion, for EBV^{EBNA2-} infections, and the widely used B95.8 EBV strain for EBV^{EBNA2+} infections. We used the immortalized Ramos B cell line instead of primary B lymphocytes as host for the infections to control for the heterogeneity of the B cell compartment. We first examined the presence and absence of EBV-encoded molecules such as EBNA2 and the Epstein–Barr virus-encoded small RNAs (EBERs) across the three cell types. As expected, we detected transcripts for EBERs only in the EBV-infected Ramos cells (both EBV^{EBNA2+} and EBV^{EBNA2-}), and we detected EBNA2 transcripts and protein only in EBV^{EBNA2+} cells (Supplemental Fig. S1). Further, no RNA-seq reads mapped to the EBV genome in the uninfected data set, whereas 7535/7764 and 4249/4423 reads mapped for EBV^{EBNA2+} replicate 1/replicate 2 and EBV^{EBNA2-} replicate 1/replicate 2, respectively.

To investigate the effect of EBNA2 on host gene expression, we identified differentially expressed genes (DEGs) using these three experimental conditions. First, we compared gene expression changes between EBV^{EBNA2+} and uninfected, which captures the effect of EBV infection on human gene expression in B cells. In total, 493 human genes were differentially expressed upon EBV^{EBNA2+} infection (Supplemental Table S1), with 290 genes up-regulated and 203 down-regulated (1.5-fold change or more, adjusted P-value < 0.05). Among these EBV-dependent differentially expressed genes, 67 of the 290 up-regulated genes and 18 of the 203 down-regulated genes were consistent with a previous study examining EBV infection in primary B cells at day 28 post-infection (P-value: 0.0208, Fisher's exact test) (Wang et al. 2019; Supplemental Table S1).

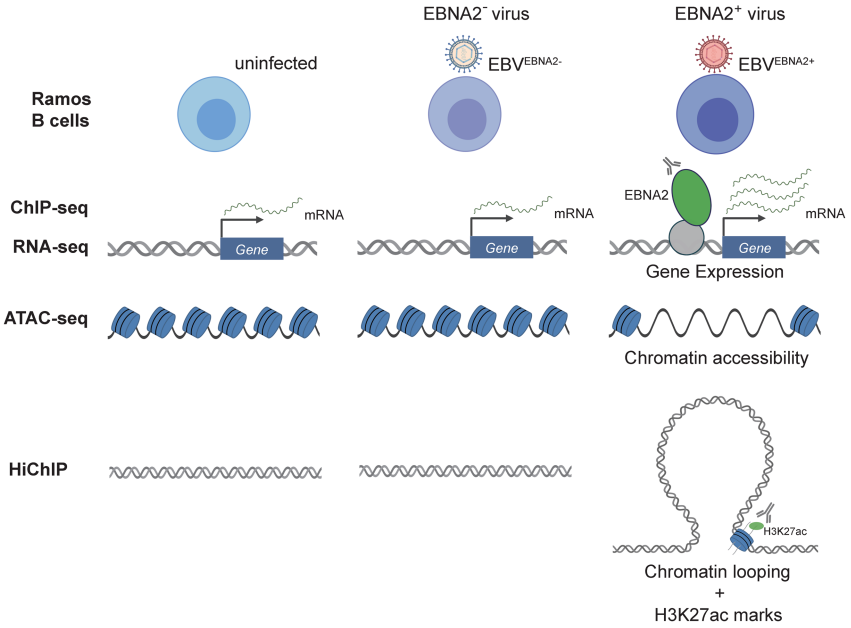

Figure 1. Schematic overview of the experimental design. Our working hypothesis is that EBNA2 alters human gene expression by rewiring the chromatin landscape. To test this hypothesis, RNA-seq, ChIP-seq, ATAC-seq, and HiChIP experiments were performed in uninfected, EBV^{EBNA2-}-infected, and EBV^{EBNA2+}-infected Ramos B cells.

Next, we identified the EBNA2-specific effects of these gene expression changes. We identified significant changes in gene expression (1.5-fold change or more, adjusted P-value < 0.05) between EBV^{EBNA2+} and uninfected cells, and between EBV^{EBNA2-} and uninfected cells (Fig. 2A–D; Supplemental Fig. S2A,B; Supplemental Table S1). This procedure identified 421 genes that are differentially expressed in the EBV^{EBNA2+} condition but not in the EBV^{EBNA2-} condition (243 up-regulated genes and 178 down-regulated genes) (Supplemental Table S1), which we designate the EBNA2 DEGs. As expected, GO Biological Process enrichment analysis for EBNA2 DEGs revealed processes involved in the immune response, including response to virus, lymphocyte activation, and cytokine production (Supplemental Fig. S3; Supplemental Table S2). Further, a significant proportion of the EBNA2 DEGs, including *CD80*, *MAP3K8*, *SLAMF1*, and *ZMIZ1*, are involved in leukocyte cell–cell adhesion (adjusted P-value: 6.03×10^{-3}) (Supplemental Table S2). Collectively, these results indicate that the expression levels of hundreds of human genes are affected by the presence of EBNA2.

EBNA2 occupies regions of the human genome proximal to genes with EBNA2-dependent expression levels

We performed ChIP-seq for EBNA2 in EBV^{EBNA2+} Ramos cells, identifying 5781 regions of the genome occupied by EBNA2 (Methods). We also performed ChIP-seq for EBNA2 in GM12878 cells, an EBV-transformed lymphoblastoid cell line. Quality control analyses indicated high data quality (Supplemental Table S3) and strong agreement between experimental replicates (Supplemental Fig. S4). We note that the FRiP score of our EBNA2 GM12878 data set is almost double the FRiP score of a publicly available EBNA2 GM12878 data set (0.036 vs. 0.0185). Our EBNA2 Ramos ChIP-seq experiment has a lower FRiP score (0.010), but this still compares favorably to the majority of publicly available virus ChIP-seq data sets (rank is 16 of 54) (Liu et al. 2020). Throughout this study, we use our RELI tool (Harley et al. 2018) to compare genomic data sets. In brief, RELI uses a simulation-based procedure to systematically gauge the significance of the intersection between a set of input genomic regions (e.g., EBNA2 ChIP-seq peaks) and each member of a large library of functional genomics experiments (e.g., published ChIP-seq or ATAC-seq peaks). Comparison of the genomic coordinates of our EBNA2 ChIP-seq data sets to published EBNA2 ChIP-seq data sets using our RELI algorithm revealed highly significant concordance (Supplemental Table S4). Likewise, our EBV^{EBNA2+} and GM12878 ChIP-seq peaks aligned significantly with published ChIP-seq peaks of established EBNA2 partners and coregulators performed in EBV-infected B cells (Zhou et al. 2015), including RBPJ, NFKB1, and EBF1 (Supplemental Table S4). As expected, we observed enrichment within our EBNA2 peaks for the DNA binding motifs of established EBNA2 partners, such as RBPJ, EBF1, and SPI1 (Supplemental Table S5). EBNA2 peaks are strongly enriched within 100 kb, 10 kb, and 5 kb of EBNA2-dependent gene transcription start sites (TSSs) (Supplemental Table S6). Collectively, these results indicate that our EBNA2 ChIP-seq experiments are of high quality.

We investigated the relationship between EBNA2 binding and gene expression changes in Ramos cells using RELI. As expected, EBV^{EBNA2+} Ramos ChIP-seq peaks were enriched within both proximal (promoter, up to 5 kb from the transcription start site: 2.7-fold enrichment, adjusted P-value: 1.13×10^{-8}) and distal (enhancer, up to 100 kb from the transcription start site: 1.5-fold enrichment, adjusted P-value: 3.35×10^{-8}) regions of EBNA2 DEGs. EBNA2 ChIP-seq peaks were more enriched near up-regulated than down-regulated genes within proximal regions (likely promoters) (3.2-fold and 2.0-fold, respectively) and distal regions (likely enhancers; 1.7-fold and 1.2-fold, respectively) (Supplemental Table S6). For example, EBNA2 ChIP-seq peaks are located in the promoter region of the EBNA2 DEG *LY9* (Supplemental Fig. S5), in agreement with a recently published finding that *LY9* gene expression is induced by EBV infection (Wang et al. 2019). LY9 protein expression levels have also been shown to be increased in the presence of SLE immune complexes (Hagberg et al. 2013), suggesting a possible role for EBNA2 in *LY9* gene regulation in lupus.

EBNA2 alters chromatin accessibility at thousands of human genomic loci

We examined the impact of EBNA2 on genome-wide chromatin accessibility by performing ATAC-seq in uninfected, EBV^{EBNA2-}, and EBV^{EBNA2+} conditions (Methods). We identified 45,207, 35,894, and 64,679 ATAC-seq peaks in these three conditions, respectively. Quality control analyses indicated high data quality (Supplemental Table S3), strong agreement between experimental replicates (Supplemental Fig. S4), and enrichment at transcription

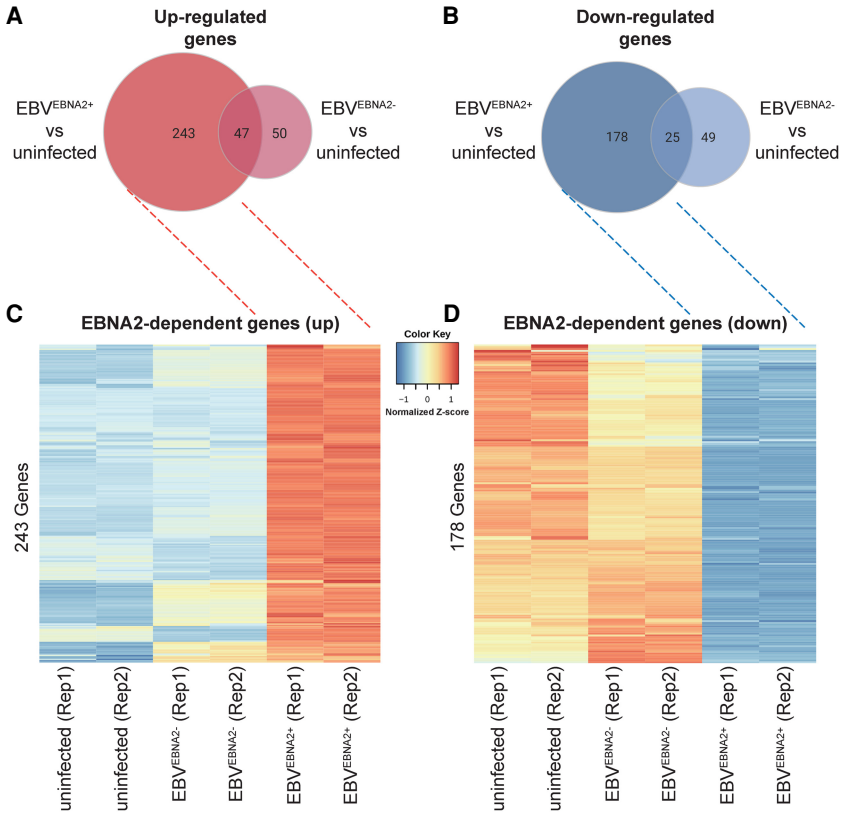

Figure 2. Differential gene expression in EBV-infected Ramos cells. Venn diagrams depicting the number of up-regulated genes (*A*) and down-regulated genes (*B*) based on comparisons between EBV^{EBNA2+} versus uninfected and EBV^{EBNA2-} versus uninfected conditions, respectively. Heatmaps depict genes that are specifically expressed higher (*C*) or lower (*D*) in EBV^{EBNA2+} cells. Values in the heatmaps indicate the normalized relative Z-score of the FPKMs across each row (i.e., the default normalization method in the R "heatmap" function) (R Core Team 2021).

start sites (Supplemental Fig. S4). These genomic regions corresponded strongly with previously published data sets performed in relevant cell types, including DNase-seq and ChIP-seq peaks for H3K27ac histone marks (Supplemental Table S7). We examined the impact of EBNA2 on chromatin accessibility by performing differential analysis using MAnorm (Shao et al. 2012) and the IDR approach (Landt et al. 2012) to discover highly reproducible changes in ATAC-seq peaks (Methods), identifying 1547 and 690 EBNA2-dependent open and closed chromatin regions, respectively (Fig. 3A; Supplemental Table S8). As expected, EBNA2 ChIP-seq peaks in Ramos EBV^{EBNA2+} cells were highly enriched within both EBNA2-dependent open chromatin accessibility gains (85 peaks; 12.4-fold enrichment; adjusted *P*-value: 4.06×10^{-104}) and EBNA2-dependent chromatin accessibility losses (321 peaks; 96.0-fold enrichment; adjusted *P*-value: 5.48×10^{-212}) (Supplemental Table S6).

We next tested the hypothesis that EBNA2 up-regulates genes by opening chromatin and down-regulates genes by closing chromatin. We used RELI to examine the significance of the intersection of EBNA2-dependent ATAC-seq peaks and genomic loci harboring EBNA2 DEGs. As expected, these analyses revealed that EBNA2-dependent open chromatin regions tend to fall proximal (within 5 kb of the TSS) to up-regulated EBNA2 DEGs (17.4-fold enriched, adjusted *P*-value: 4.30×10^{-68}), but not proximal to down-regulated EBNA2 DEGs (adjusted *P*-value: 1). Likewise, EBNA2-dependent closed chromatin showed the opposite effect, with enrichment for down-regulated EBNA2 DEGs (21.5-fold enriched, adjusted *P*-value: 2.77×10^{-50}) but not up-regulated EBNA2 DEGs (adjusted *P*-value = 1) (Supplemental Table S6). Similar results were obtained for distal (100 kb window) regions of EBNA2 DEGs. Particular TF binding motifs are preferentially enriched within EBNA2-dependent open versus closed chromatin regions. For example, Ets-like (including SPI1), TCF, and E-box motifs are much more strongly enriched in open regions, whereas ZBED, SOX, and several C_2H_2 zinc finger motifs are much more strongly enriched in closed regions (Supplemental Table S5). These results collectively reveal an important role for EBNA2 in genome-wide alteration of human chromatin accessibility.

EBNA2 extensively alters the human chromatin looping landscape

Previous reports support a role for EBNA2 in regulating the three-dimensional structure of chromatin looping (Zhao et al. 2011; McClellan et al. 2013; Jiang et al. 2017). Yet, EBNA2's roles in human chromatin looping have not been examined genome wide. Our integrative analysis of EBNA2 DEGs, EBNA2 ChIP-seq peaks, and EBNA2-specific ATAC-seq peaks revealed significant enrichment at these loci for chromatin looping factors such as CTCF, RAD21, and YY1 (Supplemental Table S4), further supporting a possible role for EBNA2 in chromatin looping alteration. To further elucidate the impact of EBNA2 on chromatin looping across the human genome, we next performed HiChIP-seq with an antibody against H3K27ac in the uninfected, EBV^{EBNA2-}, and EBV^{EBNA2+} conditions (Methods).

Analysis of the HiChIP data revealed 93,354, 131,296, and 136,689 chromatin looping interactions in the three conditions, respectively. QC analyses using HiC-Pro (Servant et al. 2015) indicate that our HiChIP experiments are of high quality. The final set of unique valid interaction pairs were between 41.4% and 51.9% of the total sequenced pairs, and the number of *trans* interactions were between 8.8% and 9.9% of the sequenced pairs (Supplemental Table S3), similar to the results obtained in the original HiChIP study (Mumbach et al. 2016). Likewise, the experimental replicates are in high agreement with one another (Supplemental Fig. S4). The full quantification of each chromatin looping event and comparisons of these events between conditions are provided in Supplemental Table S9. As expected, EBV^{EBNA2+} looping interactions significantly align (3.8-fold enrichment, *P*-value: 4.08×10^{-93}) (Methods) with data from a previously published Hi-C experiment performed in GM12878 cells (Rao et al. 2014). Furthermore, most of the EBV^{EBNA2+} HiChIP peaks coincide with publicly available H3K27ac marks (e.g., 78% of HiChIP peaks have these marks in GM19203 cells, 4.0-fold enrichment, adjusted *P*-value <1 ×

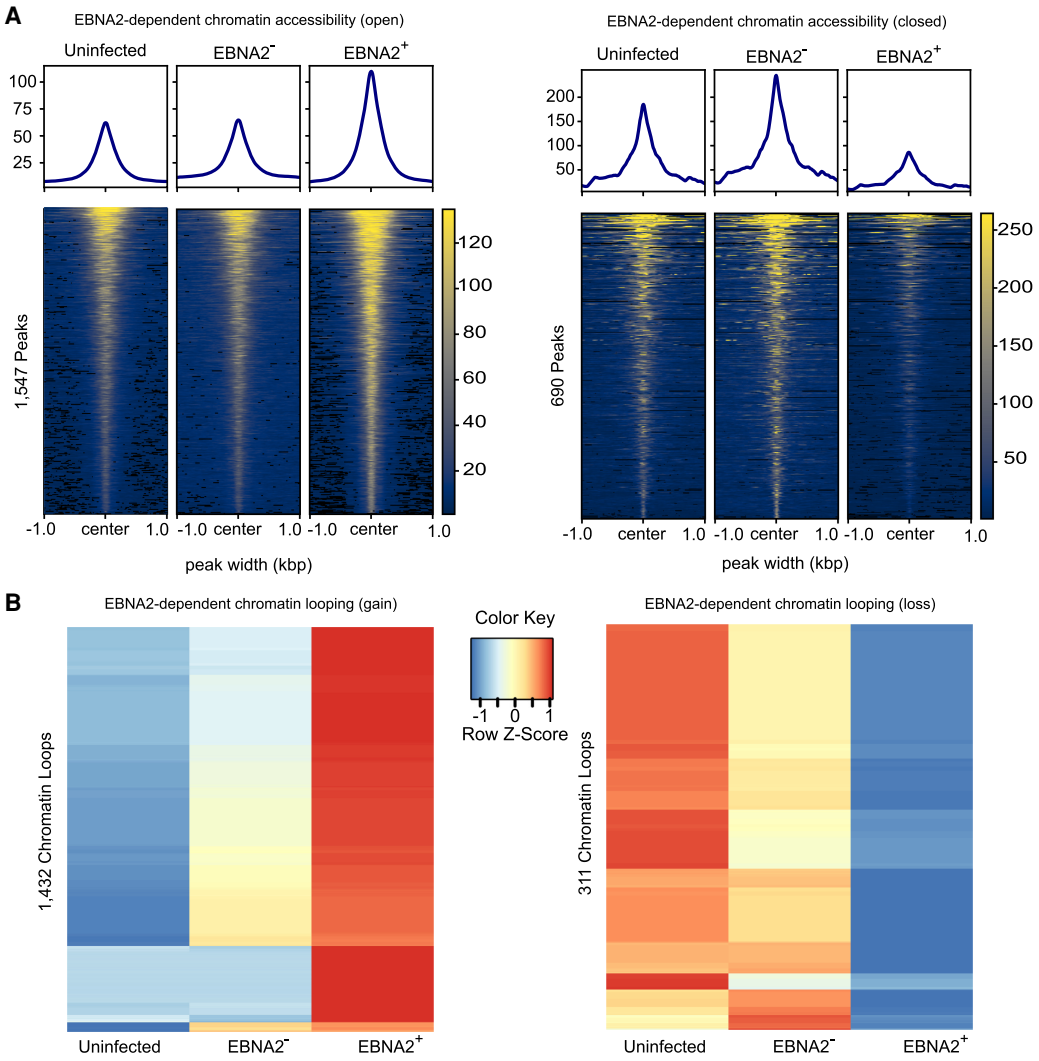

Figure 3. EBNA2-dependent chromatin accessibility and chromatin looping. (*A*) EBNA2-dependent open chromatin regions and EBNA2-dependent closed chromatin regions are depicted on the *left* and *right*, respectively. Values in the heatmaps indicate normalized read counts per genomic region and were generated using the computeMatrix tool in the deepTools package (Ramírez et al. 2016). (*B*) EBNA2-dependent chromatin loop gains (*left*) and losses (*right*). Values in the heatmaps indicate the normalized relative Z-score of the FPKMs across each row (i.e., the default normalization method in the R "heatmap" function) (R Core Team 2021).

10^{-300}) (Supplemental Table S10). ChIP-seq peaks obtained from relevant cell types for POL2RA and chromatin looping factors such as CTCF, RAD21, and YY1 significantly intersected with HiChIP loop anchors, along with active chromatin marks and DNase peaks (Supplemental Table S10). Collectively, these results indicate that our HiChIP-seq data are of high quality.

We used the HiChIP data to identify EBNA2-dependent differential chromatin looping events (Methods), identifying 1432 and 311 looping events that are significantly stronger or weaker in the presence of EBNA2, respectively (Fig. 3B; Supplemental Table S9). As expected, EBNA2-dependent "loop gains" intersect much more significantly with the promoters of up-regulated EBNA2 DEGs than with the promoters of down-regulated EBNA2 DEGs. Likewise, EBNA2-dependent "loop losses" significantly intersect with down-regulated EBNA2 DEGs, but not up-regulated EBNA2 DEGs (Supplemental Table S11). These findings support a model in which EBNA2-induced promoter interactions increase gene expression levels, whereas EBNA2-induced loss of promoter interactions decreases gene expression levels. In total, 102 newly formed EBNA2-dependent loops fall within the promoters of 70 EBNA2 DEGs (45 up-regulated and 25 down-regulated genes) (Supplemental Table S11). EBNA2-dependent gains and losses in chromatin looping were highly enriched for EBNA2 ChIP-seq peaks (12.0-fold enrichment, adjusted *P*-value: 4.77×10^{-175}; and 10.9-fold enrichment, adjusted *P*-value: 3.04×10^{-102}; EBNA2-dependent chromatin loop gains and losses, respectively) (Supplemental Table S11). EBNA2-dependent gains in chromatin looping were enriched for EBNA2-dependent chromatin accessibility gains (4.8-fold enrichment; adjusted *P*-value: 1.92×10^{-26}) but not losses (*P*-value > 0.05). Likewise, EBNA2-dependent losses in chromatin looping were enriched for chromatin accessibility losses (8.8-fold enrichment; adjusted *P*-value: 5.01×10^{-13}), but not gains (*P*-value > 0.05) (Supplemental Table S11). Fifty-eight EBNA2-dependent ATAC-seq peaks are in the promoters of EBNA2 DEGs (TSS ± 5kb). Of those, 43 EBNA2-dependent ATAC-seq peaks are within Ramos EBV^{EBNA2+} loop anchors that loop to

within 20 kb of an EBNA2 DEG. Collectively, these results indicate strong agreement between EBNA2 binding and EBNA2-dependent changes in chromatin accessibility, chromatin looping events, and gene expression. For example, we identified strong EBNA2 ChIP-seq peaks and highly EBNA2-dependent open chromatin in the promoter region of *NAALADL2-AS2*, an uncharacterized antisense long noncoding RNA that is the most highly up-regulated EBNA2 DEG (Fig. 4A). In another example, EBNA2 binds within the *SLAMF1* gene body, resulting in an EBNA2-dependent loop to the promoter of *SLAMF1*, which is one of the most strongly up-regulated EBNA2-dependent genes (Fig. 4B). The *SLAMF1* locus contains dozens of robust EBNA2-dependent chromatin looping and accessibility events involving multiple genes (Fig. 4C), revealing extensive, EBNA2-dependent rewiring of the chromatin 3D landscape at this locus.

EBNA2-dependent mechanisms significantly coincide with autoimmune disease risk loci

Previous studies (Ricigliano et al. 2015; Harley et al. 2018) have nominated an important role for EBNA2 in autoimmune and other human diseases. We therefore systematically compared the genomic locations of EBNA2-dependent mechanisms to the locations of genetic risk variants obtained from 172 published GWAS data sets (Methods). The genomic regions surrounding EBNA2 DEGs were enriched for many of the same autoimmune diseases we previously identified based on intersection of GWAS signal with EBNA2 ChIP-seq peaks (Harley et al. 2018). Specifically, 65 of the 421 EBNA2 DEGs (39 up-regulated, 26 down-regulated) have GWAS signal for autoimmune disorders within 100 kb of their transcription start site (Fig. 5A; Supplemental Table S12). Among these, 20 and 19 EBNA2 DEGs are located within SLE and MS-associated loci, respectively. In contrast, EBNA2-independent EBV DEGs (i.e., genes with higher or lower expression in both EBV^{EBNA2+} and EBV^{EBNA2-} conditions compared to uninfected) do not coincide with autoimmune disease risk loci (Supplemental Table S12), suggesting an EBNA2-specific, rather than an EBV-specific, role in autoimmune gene regulatory mechanisms.

Next, we inspected EBNA2-dependent chromatin accessibility regions for disease enrichment. Contrary to expectation, despite the vast changes in chromatin accessibility orchestrated by EBNA2, we did not identify significant intersection between EBNA2-dependent chromatin opening events and autoimmune-associated variants (Fig. 5B; Supplemental Table S12). Rather, we observed enrichment for autoimmune-associated variants within EBNA2-dependent chromatin closing events (3.6-fold enrichment, adjusted *P*-value: 7.73×10^{-6}) (Fig. 5B; Supplemental Table S12). These results prompted us to further examine the relationship between chromatin accessibility and autoimmune risk loci. To this end, we examined the significance of the intersection between autoimmune-associated variants and several types of ATAC-seq peaks: (1) constitutively open chromatin regions (i.e., peaks shared in all three conditions); (2) EBV-dependent peaks (gains and losses); (3) EBV^{EBNA2-}-dependent peaks (gains and losses); and (4) EBV^{EBNA2+}-dependent peaks (gains and losses). These analyses revealed significant intersection between autoimmune-associated variants and regions of the genome that are constitutively open in B cells (Supplemental Table S13). These results indicate that autoimmune risk variants also concentrate in regions of the genome that are already accessible for the binding of EBNA2 and other proteins before infection. Collectively, these analyses suggest that accessible chromatin before EBV infection and EBNA2-dependent chromatin closing are significant components of autoimmune risk loci but EBNA2-dependent opening of chromatin is not.

Finally, we investigated the relationship between EBNA2-altered chromatin looping interactions and autoimmune disease risk loci. This analysis revealed highly significant intersection between EBNA2-induced changes to chromatin looping and autoimmune disease risk loci. In particular, 125 newly established EBNA2-dependent chromatin loop anchors intersect autoimmune-associated variants (3.1-fold enrichment; adjusted *P*-value: 9.07×10^{-33}) (Fig. 5C; Supplemental Table S12). EBNA2-dependent loss of chromatin looping also shows significant intersection with autoimmune variants, albeit to a much lesser degree (Fig. 5C; Supplemental Table S12). Collectively, these data indicate that EBNA2-dependent alteration of long-range chromatin interactions is highly associated with autoimmune-associated genetic variants, revealing a key role for EBNA2-altered chromatin interactions in autoimmune disease etiology.

Allele-dependent EBNA2 mechanisms at autoimmune-associated risk loci

The previous analyses revealed that EBNA2-dependent chromatin alterations are significantly enriched for autoimmune-associated genetic variants. We therefore used our MARIO pipeline (Harley et al. 2018) to systematically identify autoimmune risk allele-dependent EBNA2 binding events that coincide with these EBNA2-dependent mechanisms (Methods). In brief, MARIO identifies genotype-dependent (allelic) functional genomic data (i.e., read imbalance) at genomic locations where the assayed cell contains both the reference and nonreference alleles (i.e., the genotype of the cell must be heterozygous for that specific polymorphism).

Using this approach, we discovered 32 instances of allele-dependent EBNA2 binding at autoimmune risk variants (eight in EBV^{EBNA2+} Ramos and 24 in GM12878 cells) (Supplemental Table S14), including validation in Ramos cells of the allele-dependent EBNA2 binding we previously observed for rs3794102 at the *CD44* locus in Mutu cells (Harley et al. 2018). For example, we identified strong EBNA2 allele-dependent binding in EBV^{EBNA2+} Ramos cells to an MS-associated variant (rs1250567) located in the *ZMIZ1* locus (Fig. 6). This region loops to the promoter of the short isoform of *ZMIZ1* in EBV^{EBNA2+} Ramos cells. rs1250567 is a strong eQTL for *ZMIZ1* in both EBV-immortalized lymphoblast cell lines (*P*-value: 1.76×10^{-4}) and whole blood (*P*-value: 2.21×10^{-4}; eQTL catalog) (Kerimov et al. 2021; Supplemental Table S15). *ZMIZ1* expression levels are threefold lower in EBV^{EBNA2+} Ramos cells compared to uninfected Ramos cells, consistent with a previous report by Fewings et al. (2017) describing decreased ZMIZ1 protein expression in MS patient blood samples. Collectively, our results at the *ZMIZ1* locus reveal EBNA2 and autoimmune risk allele-dependent mechanisms possibly underlying the established roles played by genetics and the environment in autoimmune diseases.

In total, 633 unique autoimmune-associated genetic variants can be implicated in at least one EBNA2-dependent mechanism (Supplemental Table S16). Among these, 24 are involved in allele-dependent EBNA2 binding, 41 are located within the promoters (TSS ± 500 bp) of EBNA2 DEGs, 46 are located within EBNA2-dependent chromatin accessibility regions, and 539 are located within EBNA2-dependent chromatin looping events. Fourteen of these variants involve multiple EBNA2-dependent mechanisms.

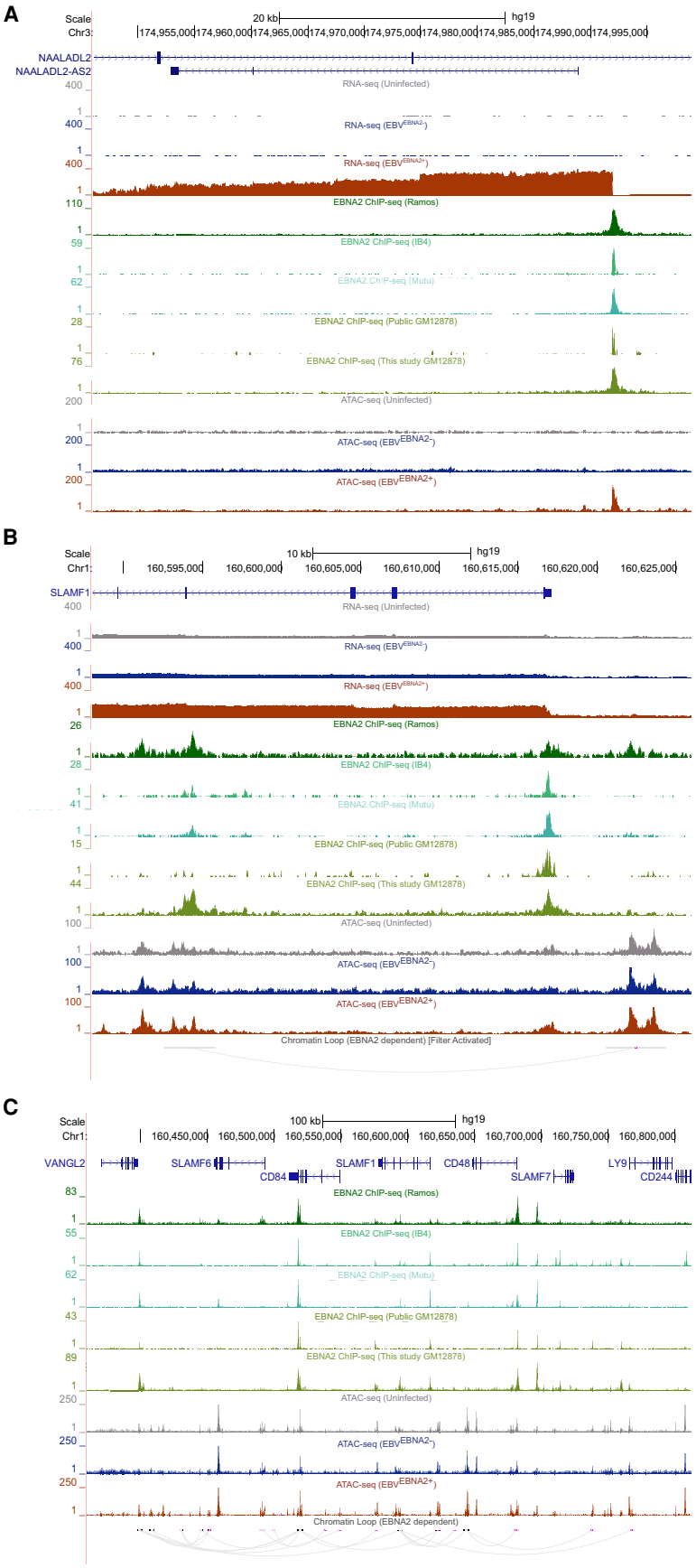

Figure 4. EBNA2-dependent alteration of the human chromatin landscape. (*A*) EBNA2 binding and EBNA2-dependent chromatin opening at the promoter of the up-regulated EBNA2 DEG *NAALADL2-AS2*, the most up-regulated EBNA2 DEG (UCSC Genome Browser screenshot [hg19]). (*B*,*C*) EBNA2-dependent alteration of chromatin looping at the *SLAMF1* locus. (*B*) EBNA2-dependent looping to the promoter of the EBNA2 DEG *SLAMF1*. Loops outside the window are not shown. (*C*) Extensive EBNA2-dependent rewiring of the chromatin looping landscape at the *SLAMF1* locus.

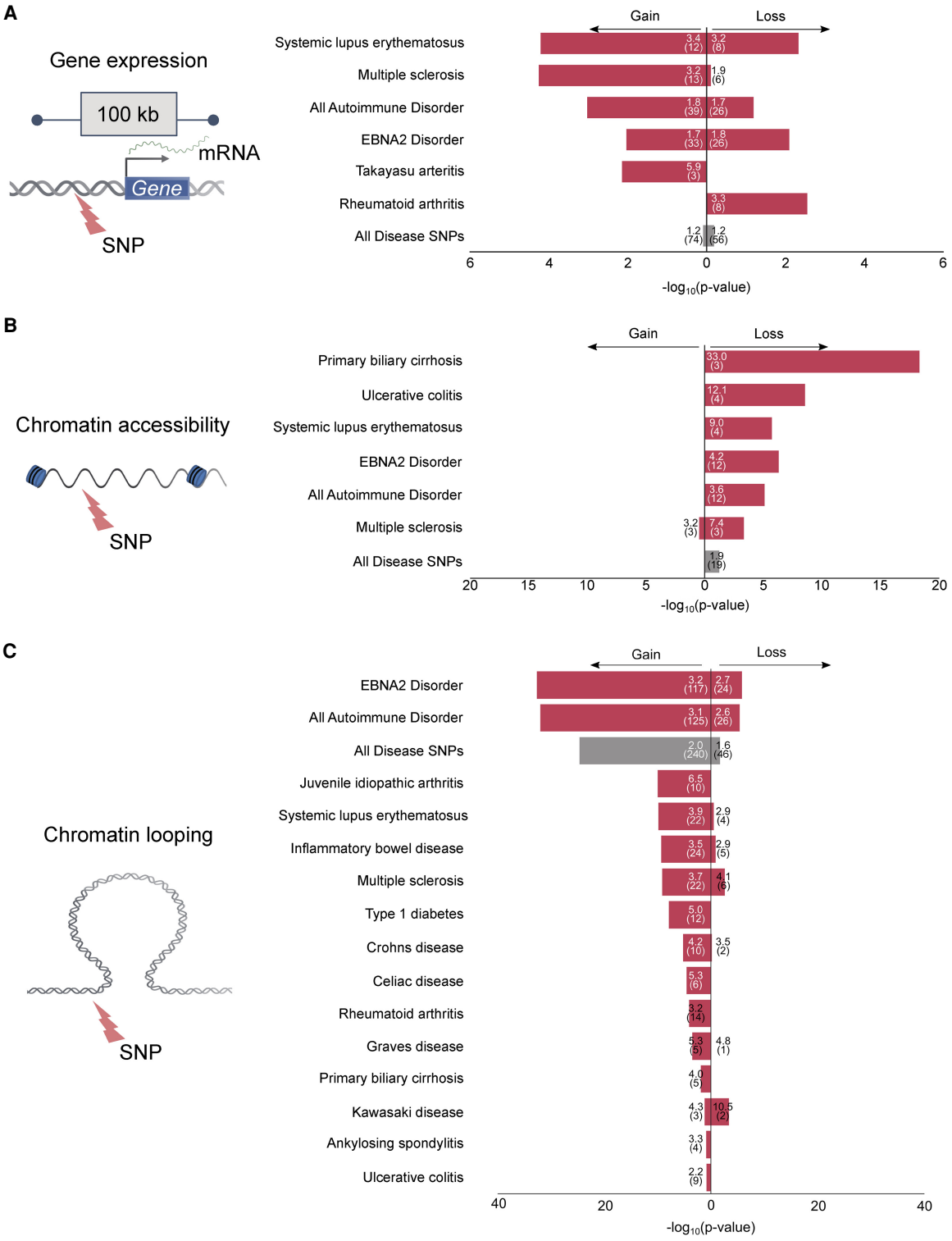

Figure 5. Intersection of EBNA2-dependent gene regulatory mechanisms and disease-associated genetic variants. The bar plots indicate the significance of the intersection (RELI negative $\log_{10}$ adjusted *P*-value). For all analyses, 19 autoimmune diseases were individually tested, along with a set of variants from all 19 autoimmune diseases ("All Autoimmune Disorders"), a set containing variants from the nine "EBNA2 Disorders" from our previous study (Harley et al. 2018), and a set containing 176 diseases and phenotypes ("All Disease SNPs"). Only diseases with at least one significant result (three or more overlaps, corrected *P*-value < 0.05) are shown. Autoimmune diseases are indicated with red bars. Fold enrichment and number of overlaps are indicated *inside* the bars. (*A*) Significant intersection between EBNA2-dependent differentially expressed genes and disease-associated variants: (Gain) up-regulated genes; (Loss) down-regulated genes. (*B*) Significant intersection between EBNA2-dependent chromatin accessibility and disease-associated variants: (Gain) newly opened chromatin; (Loss) newly closed chromatin, relative to uninfected. (*C*) Significant intersection between EBNA2-dependent chromatin looping and disease-associated variants: (Gain) new looping events; (Loss) loss of looping events.

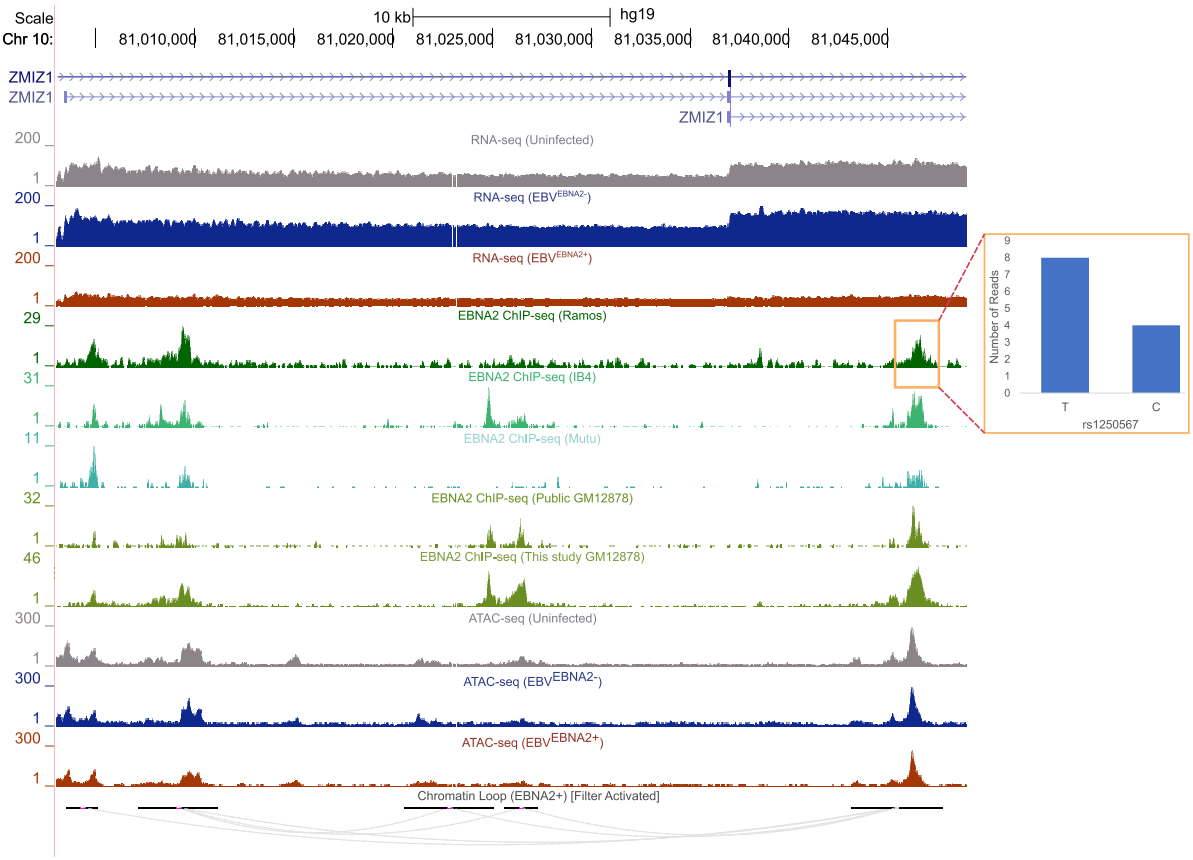

Figure 6. Allele-dependent and EBNA2-dependent effects at an autoimmune-associated genetic variant. UCSC Genome Browser screenshot (hg19) depicting EBNA2-based mechanisms at the *ZMIZ1* locus (*left*). Loops outside the window are not shown (filtered). The red box indicates the region where EBNA2 binds in an allele-dependent manner. The ratio of reads between alleles is shown as a bar plot (*right*). See text for details.

For example, the inflammatory bowel disease–associated rs630923 variant is located within the promoter of the *CXCR5* gene, which has EBNA2-dependent lower gene expression. This promoter also shows EBNA2-dependent loss of chromatin looping, providing a possible mechanism underlying the lowered expression of *CXCR5* (Supplemental Table S16). Collectively, these data implicate EBNA2 in multiple types of autoimmune disease gene regulatory mechanisms.

Discussion

In this study, we examined the mechanisms by which EBNA2, an EBV-encoded transcriptional regulator, modulates human gene regulatory programs through genome-wide perturbation of the human chromatin landscape. Our findings show that EBNA2 affects cellular gene regulation using three of the same mechanisms a host regulatory protein might use: (1) interacting with promoters and enhancers; (2) altering chromatin accessibility; and (3) forming new chromatin 3D interactions. We show that many of these mechanisms significantly intersect autoimmune-associated genetic variants, and we identify multiple EBNA2 interactions that are autoimmune risk allele-dependent.

Although it was not the focus of this study, we also identify many "EBNA2-independent" genes and regulatory elements in the human genome, which are stronger or weaker in both EBV^{EBNA2-} and EBV^{EBNA2+} cells compared to uninfected cells. These genes and elements are altered by EBV infection independently of EBNA2 and hence might involve other EBV-based regulatory molecules, such as Zta, Rta, or the EBNA3 proteins (Liu et al. 2020).

It has been extensively reported that multiple human diseases have a strong EBV-based component (Bray et al. 1983; Serafini et al. 2007; Pender and Burrows 2014) or EBNA2 component (Ricigliano et al. 2015; Harley et al. 2018). In this study, by controlling both EBV infection and the presence of EBNA2 in the EBV-infected cells, we corroborate these previous findings and identify additional gene targets and mechanisms by which EBV and EBNA2 might affect the course of these diseases. In particular, we observe significant intersection between autoimmune-associated genetic variants and EBNA2-dependent modulation of human gene expression, chromatin accessibility, and chromatin looping interactions (Fig. 5).

Previous studies have shown a key role for EBNA2 in multiple biological processes, including B cell transformation (Saha and Robertson 2019), interferon regulation (Kanda et al. 1992), and NF-kB regulation (Kim et al. 2017). In this study, we find that several genes involved in leukocyte cell–cell adhesion display EBNA2-dependent gene expression levels and regulatory mechanisms, including *NAALADL2-AS2*, *CD80*, *SLAMF1*, and *ZMIZ1*. Several of these interactions are autoimmune disease risk allele dependent. EBV infection is known to alter the expression of adhesion molecules and receptors (Zhao et al. 2006; Shannon-Lowe and Rowe

2011; Grossman et al. 2017). In particular, Fewings et al. (2017) reported a negative correlation between *ZMIZ1* expression and EBV antigen levels, consistent with the EBNA2-dependent decrease in *ZMIZ1* expression that we observe. Further, previous studies have reported elevated expression levels of adhesion molecules in SLE patients (Funauchi et al. 1993; Egerer et al. 2000) and MS patients (Elovaara et al. 2000). Together, these results support a model in which EBNA2 affects autoimmune disease onset and/or progression through the alteration of cell–cell adhesion-related gene regulatory programs.

In addition to possible EBNA2 roles in the regulation of cell–cell adhesion genes, we identified numerous strongly EBNA2-dependent genes with roles in other biological processes. Consistent with the results from Wang et al. (2019), *NAALADL2-AS2* was the gene with the highest degree of EBNA2-dependent up-regulation. *NAALADL2-AS2* is a long noncoding RNA expressed on the opposite strand of *NAALADL2*, with minimal expression across the immune compartment with the exception of naive B cells (Shay and Kang 2013). Another strongly up-regulated gene we detected is troponin T3, fast skeletal type (*TNNT3*), which is expressed across lymphocyte subsets and has been shown to interact with the EBNA2 coactivator EBNA-LP (Kempkes and Ling 2015; Rouillard et al. 2016). Solute carrier family 25 member 24 (SLC25A24) is a calcium binding carrier protein with strong EBNA2-dependent decreased gene expression. A previous study of patients with EBV-associated Burkett's lymphoma found that patient death was associated with SLC25A24 down-regulation when the tumor was EBV-positive (Kaymaz et al. 2017).

We observed widespread EBNA2-dependent chromatin looping events at a genomic locus encoding multiple members of the signaling lymphocyte activation molecule (SLAM) family, including *CD84*, *SLAMF1*, and *LY9*. SLAM family genes were previously reported to have EBV-dependent gene expression patterns (Wang et al. 2019), with *SLAMF1*, in particular, being among the most strongly up-regulated EBNA2 target genes (Maier et al. 2006). SLAM family genes play key roles in several immunological processes, including humoral responses (Ma et al. 2007), development and maintenance of immune system function (Schwartzberg et al. 2009), and cell adhesion (for review, see Cannons et al. 2011). Our new results establish a possible role for EBNA2 in the regulation of the SLAM-mediated autoimmune-related immune response.

At the *ZMIZ1* locus, we present genotype-dependent binding of EBNA2 at a disease risk variant, looping of the genetic variant to the "short isoform" promoter of *ZMIZ1*, EBNA2-dependent expression of the *ZMIZ1* "short isoform," and allele-dependent expression of *ZMIZ1* as a function of the disease risk variant genotype. Although these results are consistent with our conclusion of EBNA2-dependent allelic expression of *ZMIZ1*, it is possible that additional gene regulatory mechanisms might also mediate the expression of *ZMIZ1* and contribute to disease.

A limitation of our study design is that P3HR-1 and B95.8 strains are different genetic isolates of EBV. Therefore, there are further genetic differences between the strains in addition to the EBNA2 deletion. For example, the last two exons (45 amino acids) of EBNA-LP are also deleted in the P3HR-1 virus. However, EBV mutants with these two exons deleted can still transform primary B cells, albeit at lower frequencies (Mannick et al. 1991). Further, P3HR-1 is a well-established model system that has been widely used as an EBNA2-null strain in the field of virology for decades (Murray et al. 1988; Zimber-Strobl et al. 1991; Lee et al. 2002; Jiang et al. 2017).

In summary, our findings reveal an important role for the EBV-encoded EBNA2 regulatory protein in multiple mechanisms that ultimately affect human gene expression levels. Several of these mechanisms are allele-dependent at variants associated with autoimmune diseases such as MS and SLE. It is possible that other viral transcriptional regulators play similar mechanistic roles in other diseases. Future studies will deepen our knowledge of the mechanisms underlying virus–host interactions, and ultimately they will provide both a rationale and a foundation for therapeutic approaches targeting these interactions.

Methods

EBV infection of Ramos B cells

Wild-type B95.8 EBV (EBV^{EBNA2+}) and P3HR-1 EBV lacking EBNA2 (EBV^{EBNA2-}) were prepared from cell supernatants and cultured in 10% FBS supplemented RPMI-1640 medium for 2 wk. Viral suspension was filtered via 0.45 µm Millipore filters and cells were pelleted. The concentrated viral stocks were stored at −80°C. 2×10^6 Ramos cells (EBV Negative, ATCC CRL-1596) were infected with 1 mL viral stock based on infection optimization assays and incubated for 4 h for virus adsorption. After infection, cells were washed and cultured. After 10 passages, we confirmed the infection by morphological changes and the expression of EBNA2 viral protein levels as previously published (Harley et al. 2018).

RNA-seq

RNA was extracted, sequenced, and analyzed using standard methods (Supplemental Methods).

ChIP-seq

ChIP-seq for EBNA2 was performed in duplicate in Ramos (EBV^{EBNA2+}) and GM12878 cell lines, using standard experimental procedures (Supplemental Methods). The resulting libraries were sequenced targeting 100,000,000 unique single-end reads. We performed quality control of raw sequencing reads using FastQC (version: 0.11.2) (http://www.bioinformatics.babraham.ac.uk/projects/fastqc). All data were confirmed to pass all quality control checks (Supplemental Table S3), except for adapter sequence contents, which were removed using cutadapt (Trim Galore! version: 0.4.2) (Martin 2011). Alignment of reads to the human genome (build hg19) was performed using Bowtie 2 (Langmead and Salzberg 2012). Peaks were called using Model-based Analysis of ChIP-Seq version 2.1.1 (MACS2) (Feng et al. 2012) with the following arguments: -g hs -q 0.01. These settings were chosen from several tested parameter combinations because they yielded the best TF binding site motif enrichment *P*-values (using HOMER) for EBNA2 binding partner RBPJ. We observed strong agreement between experimental replicates (Supplemental Fig. S4). Motif enrichment for established EBNA2 partners RBPJ, EBF1, and SPI1 was slightly stronger in peaks called by pooling experimental replicate reads compared to peaks obtained using an ENCODE-like IDR-based method (Supplemental Table S5). We thus pooled the reads between the replicates and re-called peaks using MACS2 to capture as many EBNA2 binding events as possible. We also obtained publicly available EBNA2 ChIP-seq data sets (NCBI Sequence Read Archive [SRA; https://www.ncbi.nlm.nih.gov/sra] accession numbers SRX1530787 for GM12878 cells; SRX092451 for IB4 cells; and SRX290877 for Mutu cells) and called peaks using MACS2 with the following arguments: -g hs -q 0.01.

ATAC-seq

ATAC-seq was performed in duplicate in the three Ramos cell conditions using standard procedures (Supplemental Methods). FastQC was used to perform quality control (http://www.bioinformatics.babraham.ac.uk/projects/fastqc) as described above. ATAC-seq reads were aligned to the human genome (hg19) using Bowtie 2 (Langmead and Salzberg 2012), and peaks were called using MACS2 (same version and parameter settings as for our Ramos ChIP-seq) (Feng et al. 2012). We observed strong agreement between experimental replicates (Supplemental Fig. S4). We thus pooled the reads between the replicates and re-called peaks using MACS2 to capture as many open chromatin regions as possible. Differential chromatin accessibility was calculated using the MAnorm program (Shao et al. 2012) and BEDTools (Quinlan and Hall 2010). First, we determined EBV-dependent open chromatin by calculating EBV^{EBNA2+}-unique peaks compared to uninfected peaks (>1.5-fold, P-value < 0.05) using MAnorm. Next, to obtain EBNA2-dependent regions, we subtracted EBV^{EBNA2-}-unique peaks compared to uninfected using the BEDTools subtract command. To identify EBNA2-dependent closed chromatin, we first determined EBV-dependent closed chromatin by identifying uninfected-unique peaks compared to EBV^{EBNA2+} peaks, then we subtracted the uninfected-unique peaks compared to EBV^{EBNA2-} peaks. Finally, we used the IDR approach (IDR threshold of 5%) (Landt et al. 2012) to identify only highly reproducible changes in ATAC-seq peaks.

HiChIP

HiChIP libraries were prepared following Mumbach et al. (2016) (Methods). We obtained a single experimental data set for the uninfected condition and two experimental replicates for the EBV^{EBNA2-} and EBV^{EBNA2+} conditions. We used HiC-Pro (version: 2.11.0) to align reads and identify the Hi-C contact map (Servant et al. 2015). HiC-Pro was also used to perform quality control (Supplemental Table S3). Background correction, restriction site bias modeling, and looping interaction identification were performed using hichipper (version 0.7.3; https://github.com/aryeelab/hichipper) (Lareau and Aryee 2018b). We observed strong agreement between experimental replicates (Supplemental Fig. S4). We thus pooled the reads between the replicates and reanalyzed the data as described above. We identified differential looping events using the diffloop Bioconductor R package (1.6.0) (Lareau and Aryee 2018a). Briefly, to calculate EBNA2-dependent differential looping, we first determined EBV-dependent chromatin looping by comparing EBV^{EBNA2+} looping events to uninfected looping events using diffloop (>1.5-fold change, P-value < 0.05). Likewise, we also compared EBV^{EBNA2-} looping events to uninfected looping events using the same cutoffs. Then to identify EBNA2-dependent looping events, we applied diffloop again, comparing EBV^{EBNA2+}-dependent looping events to EBV^{EBNA2-}- dependent looping events, using the same cutoffs.

We calculated the significance of the intersection between chromatin looping events in the EBV^{EBNA2+} condition and looping data from GM12878 cells (Rao et al. 2014), by using a permutation test. Specifically, we randomized EBV^{EBNA2+} loop coordinates using 500 iterations of permutation. Permutations were performed by randomly sampling a gene promoter, placing one end of the loop in that promoter, and the other end of the loop the same distance away from that promoter as the "real" loop. This randomization procedure thus controls both for the looping distance and the propensity for loops to have higher densities near gene promoters. We then calculated a Z-score by comparing the distribution of randomized intersection counts to actual intersection counts.

Estimation of the significance of intersected genomic coordinates using RELI

We chose to use the hg19 genome build as our reference because many more public functional genomics data sets are available for this build compared to hg38. This choice will not affect the conclusions of this study because the average percentage of agreement between hg19 and hg38 for our data sets is very high: 95% peak agreement (ChIP-seq), 99% peak agreement (ATAC-seq), 97% anchor agreement (HiChIP), and 90% shared expressed genes (RNA-seq). Peak and loop calls are available on the study GEO page for both hg19 and hg38 coordinates.

We used the RELI method to calculate the significance of intersection between the genomic coordinates of two or more data sets. In brief, RELI calculates the overlap between the input genomic coordinates and a library of ChIP-seq-derived genomic coordinates. It then permutes the input coordinates to calculate the overlap between randomized coordinates and the library coordinates. After 2000 iterations, RELI then compares the randomized overlap to the actual overlap and calculates the significance of this overlap (Harley et al. 2018). We used a RELI library containing 1544 TF data sets, 2455 non-TF data sets, and disease-associated genetic variants (through GWAS) from 172 diseases (Harley et al. 2018). Search windows (100 kb for distal, 5 kb for promoter) were padded from the transcription start site (TSS) coordinates of EBNA2 DEGs. We ran RELI (null model: OpenChrom) with padded DEGs, EBNA2 ChIP-seq, EBNA2-dependent chromatin, and EBNA2 looping interactions. RELI output was filtered based on the number of overlaps (greater than 3) and significance (adjusted P-value < 0.05, Bonferroni correction), following our standard practices.

Identification of allele-dependent sequencing reads using MARIO

Allele-dependent behavior was identified in sequencing reads using the MARIO pipeline (Harley et al. 2018). Briefly, the MARIO pipeline identifies allele-dependent behavior by weighing (1) the imbalance between the number of reads that are mapped to each allele, (2) the total number of reads mapped at each variant, and (3) the number and consistency of available replicates. These variables are combined into a single Allelic Reproducibility Score (ARS), which reflects the degree of allelic behavior observed for the given heterozygous variant in the given data set. To identify heterozygous variants, we used genotyping array data for Ramos cells (Harley et al. 2018) and GM12878 cells. Imputation was performed using the impute2 program (Howie et al. 2009). MARIO ARS values exceeding 0.4 were considered to be allelic, following our previous study (Harley et al. 2018).

TF DNA binding motif enrichment analysis

We used the HOMER software package (Heinz et al. 2010) to calculate TF DNA binding site motif enrichment. We used a modified version of HOMER that incorporates human motifs obtained from Cis-BP build 2.0 (Weirauch et al. 2014; Lambert et al. 2019).

GWAS data set curation

We obtained GWAS data from multiple studies from the NHGRI-EBI GWAS catalog (version GWAS_catalog_v1.0.2-associations_e96_r2019-05-03) (Buniello et al. 2019). A genome-wide significance cutoff of 5×10^{-8} was used to establish the statistical significance of a variant and its association to a given disease or trait. After filtering for genome-wide association, variants were grouped based on the disease or trait reported in the publication as well as the reported ancestries. For each disease or trait,

independent loci were identified using LD-based pruning in PLINK (Purcell et al. 2007) (window size 300,000 kb, SNP shift size 100,000 kb, and $r^2 < 0.2$).

Data access

All raw and processed sequencing data generated in this study have been submitted to the NCBI Gene Expression Omnibus (GEO; https://www.ncbi.nlm.nih.gov/geo/) under accession number GSE148396. A UCSC Genome Browser session for the hg19 genome build is available at http://genome.ucsc.edu/s/ledsall/2021_EBNA2. Source code for RELI and MARIO are available on GitHub (https://github.com/WeirauchLab/RELI and https://github.com/WeirauchLab/MARIO, respectively) and as Supplemental Code.

Competing interest statement

The authors declare no competing interests.

Acknowledgments

We thank Artem Barski for maintaining robot facilities for ChIP-seq experiments; Kevin Ernst for critical input on technical issues and computational support, including servers, software packages, and data management; and Mario Pujato (AstraZeneca), Xiaoting Chen, and Xiaoming Lu for insights related to data analysis. The cartoons from Figures 1 and 5 were created using BioRender (https://BioRender.com). This study was supported by National Institutes of Health (NIH) grants R01 HG010730, R01 NS099068, R01 GM055479, and NIH Office of Research Infrastructure Programs grant U01 AI150748 (M.T.W.); R01 AR073228 and P01 AI150585 (L.C.K. and M.T.W.); R01 DK107502 and P30 AR070549 (L.C.K.); and U01 AI130830, U01 HG008666, R01 AI024717, R01 AI148276, and I01 BX001834 (J.B.H.). This study was further supported by funding from the Ohio Supercomputing Center (M.T.W.), along with funds from Cincinnati Children's Research Foundation Academic and Research Committee (ARC) and Center for Pediatric Genomics (CpG) awards (M.T.W., L.C.K., and J.B.H.) and a Cincinnati Children's Research Foundation (CCRF) Endowed Scholar Award (M.T.W.).

References

Agudelo-Romero P, Carbonell P, Perez-Amador MA, Elena SF. 2008. Virus adaptation by manipulation of host's gene expression. *PLoS One* **3:** e2397. doi:10.1371/journal.pone.0002397

Ascherio A, Munger KL. 2007. Environmental risk factors for multiple sclerosis. Part I: the role of infection. *Ann Neurol* **61:** 288–299. doi:10.1002/ana.21117

Bagert BA. 2009. Epstein-Barr virus in multiple sclerosis. *Curr Neurol Neurosci Rep* **9:** 405–410. doi:10.1007/s11910-009-0059-9

Balandraud N, Roudier J. 2018. Epstein-Barr virus and rheumatoid arthritis. *Joint Bone Spine* **85:** 165–170. doi:10.1016/j.jbspin.2017.04.011

Beagan JA, Duong MT, Titus KR, Zhou L, Cao Z, Ma J, Lachanski CV, Gillis DR, Phillips-Cremins JE. 2017. YY1 and CTCF orchestrate a 3D chromatin looping switch during early neural lineage commitment. *Genome Res* **27:** 1139–1152. doi:10.1101/gr.215160.116

Bermudez-Morales VH, Peralta-Zaragoza O, Alcocer-Gonzalez JM, Moreno J, Madrid-Marina V. 2011. IL-10 expression is regulated by HPV E2 protein in cervical cancer cells. *Mol Med Rep* **4:** 369–375. doi:10.3892/mmr.2011.429

Bochkov YA, Hanson KM, Keles S, Brockman-Schneider RA, Jarjour NN, Gern JE. 2010. Rhinovirus-induced modulation of gene expression in bronchial epithelial cells from subjects with asthma. *Mucosal Immunol* **3:** 69–80. doi:10.1038/mi.2009.109

Bookman EB, McAllister K, Gillanders E, Wanke K, Balshaw D, Rutter J, Reedy J, Shaughnessy D, Agurs-Collins T, Paltoo D, et al. 2011. Gene-environment interplay in common complex diseases: forging an integrative model—recommendations from an NIH workshop. *Genet Epidemiol* **35:** 217–225. doi:10.1002/gepi.20571

Bray PF, Bloomer LC, Salmon VC, Bagley MH, Larsen PD. 1983. Epstein-Barr virus infection and antibody synthesis in patients with multiple sclerosis. *Arch Neurol* **40:** 406–408. doi:10.1001/archneur.1983.04050070036006

Buniello A, MacArthur JAL, Cerezo M, Harris LW, Hayhurst J, Malangone C, McMahon A, Morales J, Mountjoy E, Sollis E, et al. 2019. The NHGRI-EBI GWAS Catalog of published genome-wide association studies, targeted arrays and summary statistics 2019. *Nucleic Acids Res* **47:** D1005–D1012. doi:10.1093/nar/gky1120

Çalışkan M, Baker SW, Gilad Y, Ober C. 2015. Host genetic variation influences gene expression response to rhinovirus infection. *PLoS Genet* **11:** e1005111. doi:10.1371/journal.pgen.1005111

Cannons JL, Tangye SG, Schwartzberg PL. 2011. SLAM family receptors and SAP adaptors in immunity. *Annu Rev Immunol* **29:** 665–705. doi:10.1146/annurev-immunol-030409-101302

Clyde K, Glaunsinger BA. 2010. Getting the message direct manipulation of host mRNA accumulation during gammaherpesvirus lytic infection. *Adv Virus Res* **78:** 1–42. doi:10.1016/B978-0-12-385032-4.00001-X

Deplancke B, Alpern D, Gardeux V. 2016. The genetics of transcription factor DNA binding variation. *Cell* **166:** 538–554. doi:10.1016/j.cell.2016.07.012

Dimitroulia E, Pitiriga VC, Piperaki ET, Spanakis NE, Tsakris A. 2013. Inflammatory bowel disease exacerbation associated with Epstein-Barr virus infection. *Dis Colon Rectum* **56:** 322–327. doi:10.1097/DCR.0b013e31827cd02c

Dunmire SK, Hogquist KA, Balfour HH. 2015. Infectious mononucleosis. *Curr Top Microbiol Immunol* **390**(Pt. 1): 211–240. doi:10.1007/978-3-319-22822-8_9

Egerer K, Feist E, Rohr U, Pruss A, Burmester GR, Dörner T. 2000. Increased serum soluble CD14, ICAM-1 and E-selectin correlate with disease activity and prognosis in systemic lupus erythematosus. *Lupus* **9:** 614–621. doi:10.1191/096120300678828749

Elovaara I, Ukkonen M, Leppäkynnäs M, Lehtimäki T, Luomala M, Peltola J, Dastidar P. 2000. Adhesion molecules in multiple sclerosis: relation to subtypes of disease and methylprednisolone therapy. *Arch Neurol* **57:** 546–551. doi:10.1001/archneur.57.4.546

Feng J, Liu T, Qin B, Zhang Y, Liu XS. 2012. Identifying ChIP-seq enrichment using MACS. *Nat Protoc* **7:** 1728–1740. doi:10.1038/nprot.2012.101

Fewings NL, Gatt PN, McKay FC, Parnell GP, Schibeci SD, Edwards J, Basuki MA, Goldinger A, Fabis-Pedrini MJ, Kermode AG, et al. 2017. The autoimmune risk gene ZMIZ1 is a vitamin D responsive marker of a molecular phenotype of multiple sclerosis. *J Autoimmun* **78:** 57–69. doi:10.1016/j.jaut.2016.12.006

Flavahan WA, Gaskell E, Bernstein BE. 2017. Epigenetic plasticity and the hallmarks of cancer. *Science* **357:** eaal2380. doi:10.1126/science.aal2380

Flemington E, Speck SH. 1990. Epstein-Barr virus BZLF1 *trans* activator induces the promoter of a cellular cognate gene, c-*fos*. *J Virol* **64:** 4549–4552. doi:10.1128/jvi.64.9.4549-4552.1990

Foxman EF, Iwasaki A. 2011. Genome-virome interactions: examining the role of common viral infections in complex disease. *Nat Rev Microbiol* **9:** 254–264. doi:10.1038/nrmicro2541

Funauchi M, Ohno M, Minoda M, Horiuchi A. 1993. Abnormal expression of intercellular adhesion molecule-1 on peripheral blood mononuclear cells from patients with systemic lupus erythematosus. *J Clin Lab Immunol* **40:** 115–124.

Graham SV. 2016. Human papillomavirus E2 protein: linking replication, transcription, and RNA processing. *J Virol* **90:** 8384–8388. doi:10.1128/JVI.00502-16

Grossman L, Chang C, Dai J, Nikitin PA, Jima DD, Dave SS, Luftig MA. 2017. Epstein-Barr virus induces adhesion receptor CD226 (DNAM-1) expression during primary B-cell transformation into lymphoblastoid cell lines. *mSphere* **2:** e00305-17. doi:10.1128/mSphere.00305-17

Hagberg N, Theorell J, Schlums H, Eloranta ML, Bryceson YT, Rönnblom L. 2013. Systemic lupus erythematosus immune complexes increase the expression of SLAM family members CD319 (CRACC) and CD229 (LY-9) on plasmacytoid dendritic cells and CD319 on $CD56^{dim}$ NK cells. *J Immunol* **191:** 2989–2998. doi:10.4049/jimmunol.1301022

Harley JB, James JA. 2006. Epstein-Barr virus infection induces lupus autoimmunity. *Bull NYU Hosp Jt Dis* **64:** 45–50.

Harley JB, Chen X, Pujato M, Miller D, Maddox A, Forney C, Magnusen AF, Lynch A, Chetal K, Yukawa M, et al. 2018. Transcription factors operate across disease loci, with EBNA2 implicated in autoimmunity. *Nat Genet* **50:** 699–707. doi:10.1038/s41588-018-0102-3

Heinz S, Benner C, Spann N, Bertolino E, Lin YC, Laslo P, Cheng JX, Murre C, Singh H, Glass CK. 2010. Simple combinations of lineage-determining transcription factors prime *cis*-regulatory elements required for

macrophage and B cell identities. *Mol Cell* **38:** 576–589. doi:10.1016/j.molcel.2010.05.004
Henkel T, Ling PD, Hayward SD, Peterson MG. 1994. Mediation of Epstein-Barr virus EBNA2 transactivation by recombination signal-binding protein J_κ. *Science* **265:** 92–95. doi:10.1126/science.8016657
Hindorff LA, Sethupathy P, Junkins HA, Ramos EM, Mehta JP, Collins FS, Manolio TA. 2009. Potential etiologic and functional implications of genome-wide association loci for human diseases and traits. *Proc Natl Acad Sci* **106:** 9362–9367. doi:10.1073/pnas.0903103106
Hong JY, Bentley JK, Chung Y, Lei J, Steenrod JM, Chen Q, Sajjan US, Hershenson MB. 2014. Neonatal rhinovirus induces mucous metaplasia and airways hyperresponsiveness through IL-25 and type 2 innate lymphoid cells. *J Allergy Clin Immunol* **134:** 429–439.e8. doi:10.1016/j.jaci.2014.04.020
Howie BN, Donnelly P, Marchini J. 2009. A flexible and accurate genotype imputation method for the next generation of genome-wide association studies. *PLoS Genet* **5:** e1000529. doi:10.1371/journal.pgen.1000529
Hunter DJ. 2005. Gene-environment interactions in human diseases. *Nat Rev Genet* **6:** 287–298. doi:10.1038/nrg1578
Jiang S, Zhou H, Liang J, Gerdt C, Wang C, Ke L, Schmidt SCS, Narita Y, Ma Y, Wang S, et al. 2017. The Epstein-Barr virus regulome in lymphoblastoid cells. *Cell Host Microbe* **22:** 561–573.e4. doi:10.1016/j.chom.2017.09.001
Kamen DL. 2014. Environmental influences on systemic lupus erythematosus expression. *Rheum Dis Clin North Am* **40:** 401–412, vii. doi:10.1016/j.rdc.2014.05.003
Kanda K, Decker T, Aman P, Wahlstrom M, von Gabain A, Kallin B. 1992. The EBNA2-related resistance towards α interferon (IFN-α) in Burkitt's lymphoma cells effects induction of IFN-induced genes but not the activation of transcription factor ISGF-3. *Mol Cell Biol* **12:** 4930–4936. doi:10.1128/mcb.12.11.4930-4936.1992
Kaymaz Y, Oduor CI, Yu H, Otieno JA, Ong'echa JM, Moormann AM, Bailey JA. 2017. Comprehensive transcriptome and mutational profiling of endemic Burkitt lymphoma reveals EBV type–specific differences. *Mol Cancer Res* **15:** 563–576. doi:10.1158/1541-7786.MCR-16-0305
Kempkes B, Ling PD. 2015. EBNA2 and its coactivator EBNA-LP. *Curr Top Microbiol Immunol* **391:** 35–59. doi:10.1007/978-3-319-22834-1_2
Kerimov N, Hayhurst JD, Peikova K, Manning JR, Walter P, Kolberg L, Samoviča M, Sakthivel MP, Kuzmin I, Trevanion SJ, et al. 2021. A compendium of uniformly processed human gene expression and splicing quantitative trait loci. *Nat Genet* **53:** 1290–1299. doi:10.1038/s41588-021-00924-w
Kim JH, Kim WS, Hong JY, Ryu KJ, Kim SJ, Park C. 2017. Epstein-Barr virus EBNA2 directs doxorubicin resistance of B cell lymphoma through CCL3 and CCL4-mediated activation of NF-κB and Btk. *Oncotarget* **8:** 5361–5370. doi:10.18632/oncotarget.14243
Lambert SA, Jolma A, Campitelli LF, Das PK, Yin Y, Albu M, Chen X, Taipale J, Hughes TR, Weirauch MT. 2018. The human transcription factors. *Cell* **172:** 650–665. doi:10.1016/j.cell.2018.01.029
Lambert SA, Yang AWH, Sasse A, Cowley G, Albu M, Caddick MX, Morris QD, Weirauch MT, Hughes TR. 2019. Similarity regression predicts evolution of transcription factor sequence specificity. *Nat Genet* **51:** 981–989. doi:10.1038/s41588-019-0411-1
Landt SG, Marinov GK, Kundaje A, Kheradpour P, Pauli F, Batzoglou S, Bernstein BE, Bickel P, Brown JB, Cayting P, et al. 2012. ChIP-seq guidelines and practices of the ENCODE and modENCODE consortia. *Genome Res* **22:** 1813–1831. doi:10.1101/gr.136184.111
Langmead B, Salzberg SL. 2012. Fast gapped-read alignment with Bowtie 2. *Nat Methods* **9:** 357–359. doi:10.1038/nmeth.1923
Lareau CA, Aryee MJ. 2018a. diffloop: a computational framework for identifying and analyzing differential DNA loops from sequencing data. *Bioinformatics* **34:** 672–674. doi:10.1093/bioinformatics/btx623
Lareau CA, Aryee MJ. 2018b. hichipper: a preprocessing pipeline for calling DNA loops from HiChIP data. *Nat Methods* **15:** 155–156. doi:10.1038/nmeth.4583
Lee TI, Young RA. 2013. Transcriptional regulation and its misregulation in disease. *Cell* **152:** 1237–1251. doi:10.1016/j.cell.2013.02.014
Lee JM, Lee KH, Weidner M, Osborne BA, Hayward SD. 2002. Epstein-Barr virus EBNA2 blocks Nur77-mediated apoptosis. *Proc Natl Acad Sci* **99:** 11878–11883. doi:10.1073/pnas.182552499
Liu X, Hong T, Parameswaran S, Ernst K, Marazzi I, Weirauch MT, Fuxman Bass JI. 2020. Human virus transcriptional regulators. *Cell* **182:** 24–37. doi:10.1016/j.cell.2020.06.023
Lu F, Chen HS, Kossenkov AV, DeWispeleare K, Won KJ, Lieberman PM. 2016. EBNA2 drives formation of new chromosome binding sites and target genes for B-cell master regulatory transcription factors RBP-jκ and EBF1. *PLoS Pathog* **12:** e1005339. doi:10.1371/journal.ppat.1005339
Ma CS, Nichols KE, Tangye SG. 2007. Regulation of cellular and humoral immune responses by the SLAM and SAP families of molecules. *Annu Rev Immunol* **25:** 337–379. doi:10.1146/annurev.immunol.25.022106.141651
Mahot S, Sergeant A, Drouet E, Gruffat H. 2003. A novel function for the Epstein-Barr virus transcription factor EB1/Zta: induction of transcription of the hIL-10 gene. *J Gen Virol* **84:** 965–974. doi:10.1099/vir.0.18845-0
Maier S, Staffler G, Hartmann A, Höck J, Henning K, Grabusic K, Mailhammer R, Hoffmann R, Wilmanns M, Lang R, et al. 2006. Cellular target genes of Epstein-Barr virus nuclear antigen 2. *J Virol* **80:** 9761–9771. doi:10.1128/JVI.00665-06
Mannick JB, Cohen JI, Birkenbach M, Marchini A, Kieff E. 1991. The Epstein-Barr virus nuclear protein encoded by the leader of the EBNA RNAs is important in B-lymphocyte transformation. *J Virol* **65:** 6826–6837. doi:10.1128/jvi.65.12.6826-6837.1991
Martin M. 2011. Cutadapt removes adapter sequences from high-throughput sequencing reads. *EMBnet.journal* **17:** 3. doi:10.14806/ej.17.1.200
Maurano MT, Humbert R, Rynes E, Thurman RE, Haugen E, Wang H, Reynolds AP, Sandstrom R, Qu H, Brody J, et al. 2012. Systematic localization of common disease-associated variation in regulatory DNA. *Science* **337:** 1190–1195. doi:10.1126/science.1222794
McAllister K, Mechanic LE, Amos C, Aschard H, Blair IA, Chatterjee N, Conti D, Gauderman WJ, Hsu L, Hutter CM, et al. 2017. Current challenges and new opportunities for gene-environment interaction studies of complex diseases. *Am J Epidemiol* **186:** 753–761. doi:10.1093/aje/kwx227
McClellan MJ, Wood CD, Ojeniyi O, Cooper TJ, Kanhere A, Arvey A, Webb HM, Palermo RD, Harth-Hertle ML, Kempkes B, et al. 2013. Modulation of enhancer looping and differential gene targeting by Epstein-Barr virus transcription factors directs cellular reprogramming. *PLoS Pathog* **9:** e1003636. doi:10.1371/journal.ppat.1003636
Mumbach MR, Rubin AJ, Flynn RA, Dai C, Khavari PA, Greenleaf WJ, Chang HY. 2016. HiChIP: efficient and sensitive analysis of protein-directed genome architecture. *Nat Methods* **13:** 919–922. doi:10.1038/nmeth.3999
Murray RJ, Young LS, Calender A, Gregory CD, Rowe M, Lenoir GM, Rickinson AB. 1988. Different patterns of Epstein-Barr virus gene expression and of cytotoxic T-cell recognition in B-cell lines infected with transforming (B95.8) or nontransforming (P3HR1) virus strains. *J Virol* **62:** 894–901. doi:10.1128/jvi.62.3.894-901.1988
North KE, Howard BV, Welty TK, Best LG, Lee ET, Yeh JL, Fabsitz RR, Roman MJ, MacCluer JW. 2003. Genetic and environmental contributions to cardiovascular disease risk in American Indians: the strong heart family study. *Am J Epidemiol* **157:** 303–314. doi:10.1093/aje/kwf208
Pender MP, Burrows SR. 2014. Epstein-Barr virus and multiple sclerosis: potential opportunities for immunotherapy. *Clin Transl Immunology* **3:** e27. doi:10.1038/cti.2014.25
Pich D, Mrozek-Gorska P, Bouvet M, Sugimoto A, Akidil E, Grundhoff A, Hamperl S, Ling PD, Hammerschmidt W. 2019. First days in the life of naive human B lymphocytes infected with Epstein-Barr virus. *mBio* **10:** e01723-19. doi:10.1128/mBio.01723-19
Purcell S, Neale B, Todd-Brown K, Thomas L, Ferreira MAR, Bender D, Maller J, Sklar P, de Bakker PIW, Daly MJ, et al. 2007. PLINK: a tool set for whole-genome association and population-based linkage analyses. *Am J Hum Genet* **81:** 559–575. doi:10.1086/519795
Quinlan AR, Hall IM. 2010. BEDTools: a flexible suite of utilities for comparing genomic features. *Bioinformatics* **26:** 841–842. doi:10.1093/bioinformatics/btq033
Ramírez F, Ryan DP, Grüning B, Bhardwaj V, Kilpert F, Richter AS, Heyne S, Dündar F, Manke T. 2016. deepTools2: a next generation web server for deep-sequencing data analysis. *Nucleic Acids Res* **44:** W160–W165. doi:10.1093/nar/gkw257
Rao SS, Huntley MH, Durand NC, Stamenova EK, Bochkov ID, Robinson JT, Sanborn AL, Machol I, Omer AD, Lander ES, et al. 2014. A 3D map of the human genome at kilobase resolution reveals principles of chromatin looping. *Cell* **159:** 1665–1680. doi:10.1016/j.cell.2014.11.021
R Core Team. 2021. *R: a language and environment for statistical computing*. R Foundation for Statistical Computing, Vienna. https://www.R-project.org/.
Ricigliano VA, Handel AE, Sandve GK, Annibali V, Ristori G, Mechelli R, Cader MZ, Salvetti M. 2015. EBNA2 binds to genomic intervals associated with multiple sclerosis and overlaps with vitamin D receptor occupancy. *PLoS One* **10:** e0119605. doi:10.1371/journal.pone.0119605
Rochford R, Moormann AM. 2015. Burkitt's lymphoma. *Curr Top Microbiol Immunol* **390:** 267–285. doi:10.1007/978-3-319-22822-8_11
Rouillard AD, Gundersen GW, Fernandez NF, Wang Z, Monteiro CD, McDermott MG, Ma'ayan A. 2016. The harmonizome: a collection of processed datasets gathered to serve and mine knowledge about genes and proteins. *Database (Oxford)* **2016:** baw100. doi:10.1093/database/baw100
Saha A, Robertson ES. 2019. Mechanisms of B-cell oncogenesis induced by Epstein-Barr virus. *J Virol* **93:** e00238-19. doi:10.1128/JVI.00238-19

Schoenfelder S, Fraser P. 2019. Long-range enhancer-promoter contacts in gene expression control. *Nat Rev Genet* **20:** 437–455. doi:10.1038/s41576-019-0128-0

Schwartzberg PL, Mueller KL, Qi H, Cannons JL. 2009. SLAM receptors and SAP influence lymphocyte interactions, development and function. *Nat Rev Immunol* **9:** 39–46. doi:10.1038/nri2456

Serafini B, Rosicarelli B, Franciotta D, Magliozzi R, Reynolds R, Cinque P, Andreoni L, Trivedi P, Salvetti M, Faggioni A, et al. 2007. Dysregulated Epstein-Barr virus infection in the multiple sclerosis brain. *J Exp Med* **204:** 2899–2912. doi:10.1084/jem.20071030

Servant N, Varoquaux N, Lajoie BR, Viara E, Chen CJ, Vert JP, Heard E, Dekker J, Barillot E. 2015. HiC-Pro: an optimized and flexible pipeline for Hi-C data processing. *Genome Biol* **16:** 259. doi:10.1186/s13059-015-0831-x

Shannon-Lowe C, Rowe M. 2011. Epstein-Barr virus infection of polarized epithelial cells via the basolateral surface by memory B cell-mediated transfer infection. *PLoS Pathog* **7:** e1001338. doi:10.1371/journal.ppat.1001338

Shao Z, Zhang Y, Yuan GC, Orkin SH, Waxman DJ. 2012. MAnorm: a robust model for quantitative comparison of ChIP-Seq data sets. *Genome Biol* **13:** R16. doi:10.1186/gb-2012-13-3-r16

Shay T, Kang J. 2013. Immunological genome project and systems immunology. *Trends Immunol* **34:** 602–609. doi:10.1016/j.it.2013.03.004

Sullivan KD, Galbraith MD, Andrysik Z, Espinosa JM. 2018. Mechanisms of transcriptional regulation by p53. *Cell Death Differ* **25:** 133–143. doi:10.1038/cdd.2017.174

Tam V, Patel N, Turcotte M, Bossé Y, Paré G, Meyre D. 2019. Benefits and limitations of genome-wide association studies. *Nat Rev Genet* **20:** 467–484. doi:10.1038/s41576-019-0127-1

Vockerodt M, Cader FZ, Shannon-Lowe C, Murray P. 2014. Epstein-Barr virus and the origin of Hodgkin lymphoma. *Chin J Cancer* **33:** 591–597. doi:10.5732/cjc.014.10193

Wang L, Grossman SR, Kieff E. 2000. Epstein–Barr virus nuclear protein 2 interacts with p300, CBP, and PCAF histone acetyltransferases in activation of the LMP1 promoter. *Proc Natl Acad Sci* **97:** 430–435. doi:10.1073/pnas.97.1.430

Wang C, Li D, Zhang L, Jiang S, Liang J, Narita Y, Hou I, Zhong Q, Zheng Z, Xiao H, et al. 2019. RNA sequencing analyses of gene expression during Epstein-Barr virus infection of primary B lymphocytes. *J Virol* **93:** e00226-19. doi:10.1128/JVI.00226-19

Weintraub AS, Li CH, Zamudio AV, Sigova AA, Hannett NM, Day DS, Abraham BJ, Cohen MA, Nabet B, Buckley DL, et al. 2017. YY1 is a structural regulator of enhancer-promoter loops. *Cell* **171:** 1573–1588.e28. doi:10.1016/j.cell.2017.11.008

Weirauch MT, Yang A, Albu M, Cote AG, Montenegro-Montero A, Drewe P, Najafabadi HS, Lambert SA, Mann I, Cook K, et al. 2014. Determination and inference of eukaryotic transcription factor sequence specificity. *Cell* **158:** 1431–1443. doi:10.1016/j.cell.2014.08.009

Wood CD, Veenstra H, Khasnis S, Gunnell A, Webb HM, Shannon-Lowe C, Andrews S, Osborne CS, West MJ. 2016. *MYC* activation and *BCL2L11* silencing by a tumour virus through the large-scale reconfiguration of enhancer-promoter hubs. *eLife* **5:** e18270. doi:10.7554/eLife.18270

Wu DY, Krumm A, Schubach WH. 2000. Promoter-specific targeting of human SWI-SNF complex by Epstein-Barr virus nuclear protein 2. *J Virol* **74:** 8893–8903. doi:10.1128/JVI.74.19.8893-8903.2000

Zhao B, Maruo S, Cooper A, Chase Michael R., Johannsen E, Kieff E, Cahir-McFarland E. 2006. RNAs induced by Epstein–Barr virus nuclear antigen 2 in lymphoblastoid cell lines. *Proc Natl Acad Sci* **103:** 1900–1905. doi:10.1073/pnas.0510612103

Zhao B, Zou J, Wang H, Johannsen E, Peng CW, Quackenbush J, Mar JC, Morton CC, Freedman ML, Blacklow SC, et al. 2011. Epstein-Barr virus exploits intrinsic B-lymphocyte transcription programs to achieve immortal cell growth. *Proc Natl Acad Sci* **108:** 14902–14907. doi:10.1073/pnas.1108892108

Zhou H, Schmidt SC, Jiang S, Willox B, Bernhardt K, Liang J, Johannsen EC, Kharchenko P, Gewurz BE, Kieff E, et al. 2015. Epstein-Barr virus oncoprotein super-enhancers control B cell growth. *Cell Host Microbe* **17:** 205–216. doi:10.1016/j.chom.2014.12.013

Zimber-Strobl U, Suentzenich KO, Laux G, Eick D, Cordier M, Calender A, Billaud M, Lenoir GM, Bornkamm GW. 1991. Epstein-Barr virus nuclear antigen 2 activates transcription of the terminal protein gene. *J Virol* **65:** 415–423. doi:10.1128/jvi.65.1.415-423.1991

Received April 15, 2020; accepted in revised form October 7, 2021.